Available online at www.sciencedirect.com

ScienceDirect

Ceramics International 40 (2014) 331–339

CERAMICS INTERNATIONAL

www.elsevier.com/locate/ceramint

Evolution of remnant state variables and linear material properties in ferroelectric ceramics during compressive loading and unloading

Dae Won Ji, Sang-Joo Kim*

Department of Mechanical and Information Engineering, University of Seoul, Dongdaemun-gu, Seoul 130-743, Republic of Korea

Received 6 May 2013; received in revised form 14 May 2013; accepted 8 June 2013
Available online 14 June 2013

Abstract

A pre-poled lead titanate zirconate (PZT) cube specimen was subjected to impulsive compression stress with increasing amplitude. Linear material properties were evaluated graphically from the measured responses. The material properties were plotted versus relative remnant polarization and fitted by quadratic curves. Then the specimen was subjected to compressive creep loading and unloading of various constant magnitudes. The linear material properties obtained from impulsive stress loading were used to calculate the evolutions of remnant state variables and material properties during the compressive creep loading and unloading. The magnitudes of polarization and strains that were induced and recovered during the creep loading and unloading were plotted and discussed.

Keywords: Ferroelectric; Compressive stress; Switching; Remnant; Linear moduli

1. Introduction

Thanks to strong electromechanical coupling, prompt response, low power consumption, and many other excellent characteristics, piezoelectric ceramics such as lead titanate zirconate (PZT) have been used for various types of actuators and sensors. In these applications, the materials are often subjected to compressive stress large enough to cause unnecessary domain switching in the materials. The domain switching changes the internal structure of the materials and thus the characteristics of the materials, deteriorating the performance of piezoelectric devices. Therefore, it is very important to take the nonlinear behavior of the materials by strong compressive stress into consideration when selecting piezoelectric materials.

Constitutive modeling for nonlinear behavior of ferroelectric ceramic materials has been investigated by researchers [1–3]. In addition to the theoretical study, much experimental work has been made to understand the nonlinear behavior of the materials. Nonlinear electromechanical coupling behavior at room temperature had been measured and discussed by Cao and Evans [4] and Lynch [5]. Tensile creep behavior of ferroelectric ceramics at room temperature had been measured and reported [6,7]. Room-temperature ferroelastic switching and creep behavior under electric field and compressive stress had been investigated [8,9]. The change of Young's modulus of initially unpoled and pre-poled soft PZT material under compressive stress was studied using the partial unloading method, and it was found that Young's modulus increased with compressive stress [10]. In electric field and compressive stress loading experiments on non-poled and poled PZT ceramic, Zhou et al. [11] separated reversible and irreversible parts of total measured responses by evaluating the evolution of linear material properties, and they found that longitudinal and transverse irreversible strains changed significantly during both loading and unloading processes. Selten et al. [12] observed constant permittivity and linear dependency of piezoelectric coefficient on remnant polarization in a PZT ceramic under unipolar electrical loading; Liu and Huber [13] calculated the evolutions of linear elastic, dielectric, and piezoelectric moduli in a ferroelectric ceramic under electro-mechanical loading at room temperature. Webber et al. [14] measured and characterized the nonlinear switching behavior of soft lead zirconate titanate induced by compressive stress at elevated temperatures, observing strong temperature dependency of ferroelastic switching. The evolutions of linear

*Corresponding author. Tel.: +82 2 6490 2387; fax: +82 2 6490 2384.
E-mail address: sangjookim@gmail.com (s.-J. Kim).

0272-8842/$ - see front matter © 2013 Elsevier Ltd and Techna Group S.r.l. All rights reserved.
http://dx.doi.org/10.1016/j.ceramint.2013.06.006

materials and remnant state variables had been calculated from measured total responses at high temperatures as well as room temperature. Thermal expansion and pyroelectric coefficients had been observed to depend linearly on remnant polarization in a PZT wafer [15]; piezoelectric coefficients were given as a function of remnant polarization and temperature [16,17]. Comparison of polarization hysteresis and strain butterfly loops at room and high temperatures had been made by calculating remnant polarization and remnant strain [18]. Temperature-dependent ferroelastic behavior of ferroelectric ceramics at room and high temperatures was investigated and the evolutions of linear material properties at different temperatures were analyzed by introducing so-called relative remnant polarization [19]. A poled PZT cube was subjected to constant compressive stress of various magnitudes at four different room and high temperatures, and the evolutions of linear material properties and remnant state variables were calculated. Longitudinal and transverse remnant strains were shown to depend linearly on relative remnant polarization [20].

In present study, a poled PZT cube specimen is subjected to impulsive compression stress with increasing amplitude, and polarization and strain responses are measured during the impulsive loading. From the measured electric displacement and strains, piezoelectric coefficient and compliance coefficients are evaluated by a graphical method and plotted versus relative remnant polarization. Quadratic functions are proposed to fit the dependence of linear material properties on relative remnant polarization. Next, constant compressive stress of various magnitudes is applied to the specimen for a period of time. The stress is then removed and the specimen is left unstressed for the same period of time. During the total creep loading and unloading, electric displacement and strains are measured. Using the quadratic dependence of linear material properties on relative remnant polarization, the evolutions of remnant state variables and linear material properties during compressive creep loading and unloading are calculated. The behavior of recovered polarization and strains during the unloading period of compressive stress is calculated and discussed.

2. Experiment

The specimen that is used for experiments is a commercially available soft PZT rectangular parallelepiped (PZT5H1, Morgan Technical Ceramics, UK) of dimensions10 mm × 10 mm × 12 mm. It has been developed for applications that require high electromechanical activity and high dielectric constant, such as hydrophones, sound detectors, accelerometers, flow detectors and flow meters. The specimen PZT ceramic is electroded on the 10 mm × 10 mm faces and poled along the 12 mm direction. The 12 mm direction is referred to as longitudinal direction and designated as x_3; two mutually orthogonal directions perpendicular to x_3 are called transverse directions and designated as x_1 and x_2, respectively. The three mutually orthogonal directions x_1, x_2 and x_3 are also often called as 1, 2, and 3 directions, respectively. According to manufacturing company, the Curie point of the material is 200 °C, the density is 7400 kg m^{-3}, the coupling factor is $k_p=0.60$, the piezoelectric charge coefficients are $d_{31}=-250\times10^{-12}$ mV^{-1} and $d_{33}=620\times10^{-12}$ mV^{-1}, and the elastic compliance coefficients at constant electric field $s_{33}=21.9\times10^{-12}$ m^2 N^{-1}, $s_{11}=17.7\times10^{-12}$ m^2 N^{-1}, and $s_{12}=-5.7\times10^{-12}$ m^2 N^{-1}.

In present paper, two different types of compressive stress are applied to a poled PZT specimen at room temperature. First, impulsive compression stress with gradually increasing amplitude is applied to the specimen. A typical impulsive stress is shown in Fig. 2(a), where the amplitude of stress impulse increases from −10 MPa to −500 MPa. As will be explained below, a preload of −5 MPa is included in the stress amplitudes. In the impulse loading and unloading, stress increases and decreases at the fastest loading rate of 10 MPa s^{-1} available for the Instron 5869 machine. After both loading and unloading are finished, stress remains constant for 5 s. Longitudinal electric displacement and longitudinal and transverse strains are measured and recorded, which are used to evaluate the evolution of linear material properties during the ferroelastic switching by a graphical method. Next, constant compressive stresses of various magnitudes are applied to the specimen in the longitudinal direction of the specimen. Eight magnitudes of applied compressive stress are 20, 30, 50, 70, 100, 150, 300, and 500 MPa. A typical stress loading–unloading cycle is as follows. In the loading part, the magnitude of compressive stress increases at a slow rate of 0.5 MPa s^{-1}. Then the stress remains constant at the target level for 500 s. In the subsequent unloading part, stress decreases at the same slow rate of 0.5 MPa s^{-1}. After complete unloading, the specimen is left at zero stress for another 500 s. Because of a preloaded stress, the zero stress here is actually −5 MPa. During the whole loading and unloading cycle of compressive stress, electric displacement in x_3 direction D_3 and extensional strains in x_1 and x_3 directions S_1 and S_3 are measured and recorded. For all the eight compressive experiments, only one specimen is used. After each experiment, electric field of magnitude 1.0 MV m^{-1} is applied in $-x_3$ direction for 600 s to restore the same initial poled state. Then, after removing the electric field, the specimen is under no electric field for another 600 s. The restored initial poled state is the state represented by the polarization value of −.52 C m^{-2}. A pre-stress of −5 MPa is then applied to stabilize the initial polarization state. After another 600 s under the preload of −5 MPa, polarization is reduced to −0.50 Cm^{-2}. Thus the eight stress levels from −20 MPa to −500 MPa include the preloaded stress −5 MPa. Then, strains are set to be zero, and now it is ready to begin compressive creep loading and unloading experiments. To verify the restored poled state, several experiments at the same stress level are repeated. No significant history dependence of material responses is observed, implying that the restored poled state is sufficiently close to the initial poled state.

A schematic diagram of an experimental setup is shown in Fig. 1. The bottom face of a PZT specimen that is poled downward is in contact with the top face of steel fixture to which applied high voltage is connected. A Teflon jig with a square hole in its center, which has excellent insulation, is used as an insulating material between high voltage sources and strain gauges. Electric displacement in longitudinal direction is measured using a Sawyer–Tower bridge, where a reference capacitor (metalized polypropylene capacitor) of capacitance 100 μF is connected to the specimen in series. This is 1000

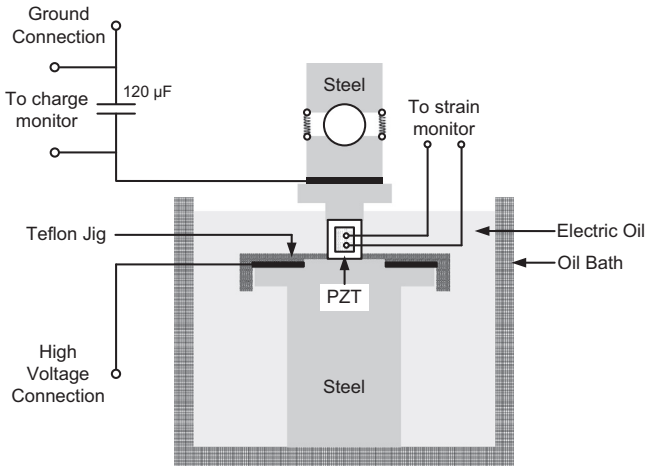

Fig. 1. Schematic experimental setup for measuring electric displacement and strains of a PZT ceramic cube under compressive stress.

times as large as the PZT specimen capacitance 0.1 μF. The voltage across the reference capacitor is measured by a Keithley 6514 electrometer. Discharge circuits are added to the system to remove the charges accumulated in the PZT specimen and the reference capacitor during experiments. When compressive stress is applied parallel to the poling x_3 direction of the specimen, it remains isotropic with respect to the poling axis, resulting in the same values of transverse strains in both x_1 and x_2 directions. Thus, in present compressive experiments, extensional strains only in x_3 and x_1 directions are measured by one biaxial strain gauge attached at the center of one of four side faces. To check bending effect during compressive loading, two biaxial strain gauges are attached on each of two parallel sides of the specimen. Measured strains from the two strain gauges did not show any significant difference and bending effect was negligible. In addition, strains measured on two adjacent orthogonal side faces have a negligible difference, too. These preliminary studies justify using only one biaxial strain gauge in a side face. The used biaxial strain gauges are fully encapsulated constantan strain gauges (WA-03-062TT-350, VISHAY, Germany). Experimental data are collected at the rate of 100 Hz. All equipment output signals pass through a data acquisition board (PCI 6221, National Instruments, TX, USA) and are manipulated using a LABVIEW software.

3. Results and discussion

3.1. Evolution of material properties and remnant state variables during impulsive stress cycles

In present section, the evolutions of material properties and remnant state variables are calculated from measured material responses to impulsive compression stress with gradually increasing amplitude. The compression impulses of magnitudes between −10 MPa and −500 MPa are shown in Fig. 2(a); and measured electric displacement D_3, longitudinal strain S_3, and transverse strain S_1 in Fig. 2(b) and (c), respectively. The impulsive stress is applied and removed at 10 MPa s^{-1}, which is the fastest rate available for the Instron machine. Linear material properties are evaluated at the beginning instant of impulsive unloading, where the amount of switching is so small that the measured response is only due to linear piezoelectric effect. Exemplary tangential straight lines on electric displacement and strain curves drawn at the beginning instant of unloading are shown for −60 MPa in Fig. 2(b) and (c), respectively. The slopes of the straight lines are, respectively, equal to $1/d_{33}$, $1/s_{33}$, and $1/s_{13}$. Thus piezoelectric coefficient d_{33} and elastic compliance coefficients s_{33}, s_{13} are evaluated from the slopes of the tangential straight lines. The values of remnant state variables P_3^R, S_3^R, and S_1^R, at which linear material properties are evaluated, are obtained from the intersections of the straight lines with horizontal axes, as indicated by arrows in the figures.

The measured strain responses in Fig. 2(c) during impulsive stress loading are plotted in the S_3 versus S_1 plane in Fig. 2(d). Interestingly, it is observed that the S_3–S_1 curves in the figure are composed of two straight parts with different slopes. The magnitude of slope is larger for the right part of the curves $-1000\times10^{-6} < S_3$ than that for the left part $S_3 < -2500\times10^{-6}$. The right part corresponds to relatively small magnitudes of compressive stress in the initial period of loading. The most active switching is expected to occur in this part of the curves, and the slope of the curve there is called switching-induced Poisson's ratio ν_s. Evaluating the slope for the smallest five stress impulses in Fig. 2(a), the average value of ν_s is found to be 0.480, which is very close to 0.476 obtained for the same PZT specimen by Kim and Ji [20]. On the other hand, the slope of S_3–S_1 curves in the left part $S_3 < -2500\times10^{-6}$ is associated mainly with elastic deformation, where the magnitude of stress is so large that the amount of switching at the beginning instant of unloading is negligible. Thus the slope of the curves in the left region is numerically equal to elastic Poisson's ratio ν_{13}. From the strain responses to the largest five stress impulses in Fig. 2(a), ν_{13} is found to be 0.305, which is a common value for elastic Poisson's ratio. Fig. 2(e) shows the evolutions of longitudinal and transverse remnant strains S_3^R and S_1^R plotted versus relative remnant polarization P_3^R/P_{3sat}^R, the former represented by solid circle symbols and the latter by solid square ones. Relative remnant polarization P_3^R/P_{3sat}^R is obtained by dividing remnant polarization P_3^R by saturated (or poled) remnant polarization P_{3sat}^R. P_{3sat}^R represents the magnitude of remnant polarization at a poled state. It is observed in the figure that both S_3^R and S_1^R are linearly proportional to P_3^R/P_{3sat}^R, which is coincident exactly with the observation of Kim and Ji [20].

All estimated values of piezoelectric coefficient d_{33} and elastic compliance coefficients s_{33}, s_{13} are plotted versus relative remnant polarization P_3^R/P_{3sat}^R in Fig. 3(a) and (b), respectively. A quick glance at the figures shows that both piezoelectric coefficient d_{33} and compliance coefficients s_{33}, s_{13} depend nearly quadratically on P_3^R/P_{3sat}^R. The magnitude of d_{33} decreases with increasing P_3^R/P_{3sat}^R, finally saturated to zero at sufficiently large compressive stresses, as expected. The magnitudes of s_{33} and s_{13} also decrease with P_3^R/P_{3sat}^R, quadratically approaching nonzero finite values as shown in Fig. 3(b). The dependence of linear

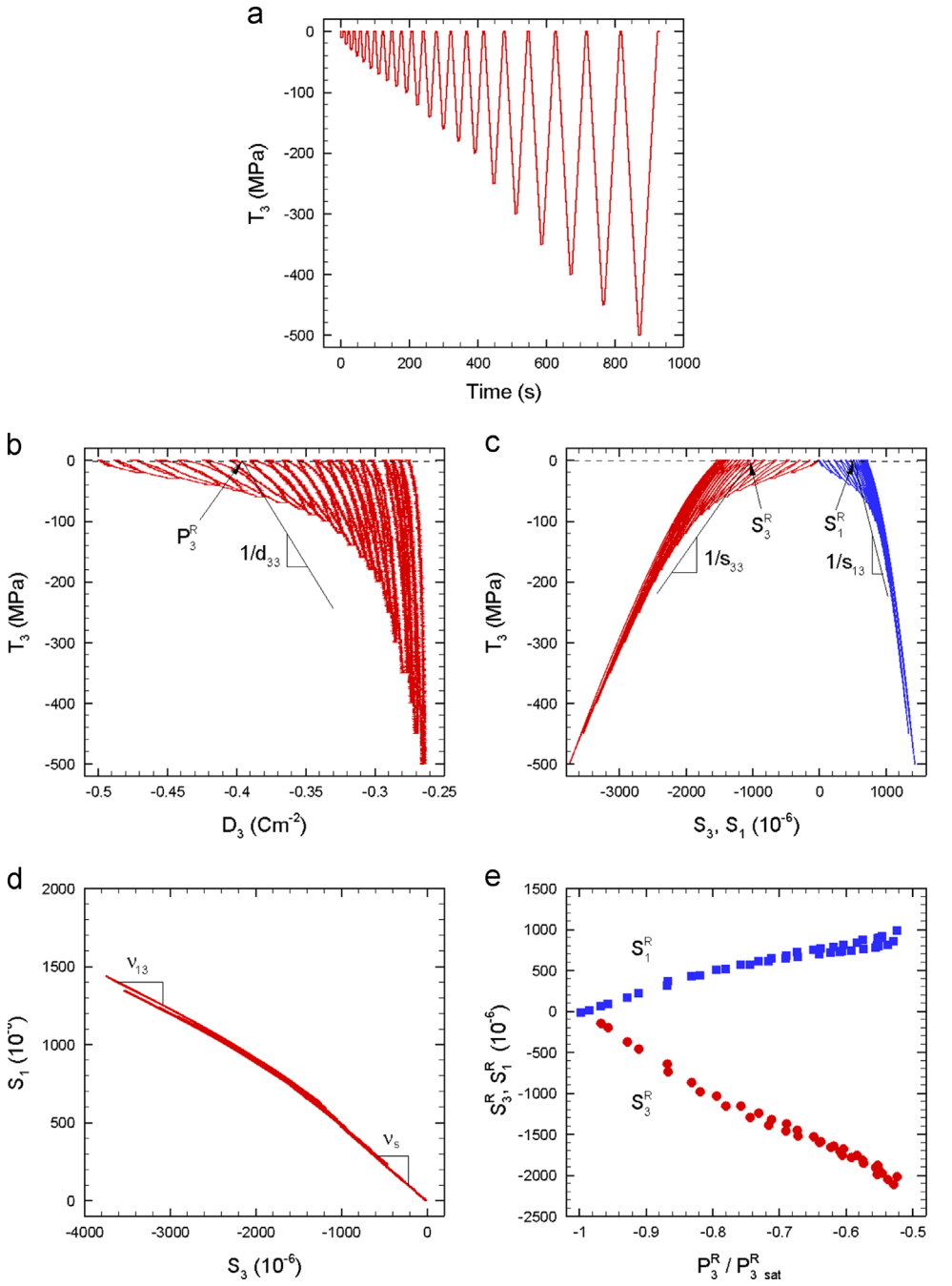

Fig. 2. Measured electric displacement and strains during impulsive compression stress with gradually increasing amplitude: (a) stress T_3 versus time, (b) stress T_3 versus electric displacement D_3, (c) stress T_3 versus strains S_3, S_1, (d) transverse strain S_1 versus longitudinal strain S_3, and (e) remnant strains S_3^R, S_1^R versus relative remnant polarization P_3^R/P_{3sat}^R plots.

material properties on P_3^R/P_{3sat}^R is similar to that observed by Kim and Ji [20], where d_{33}, s_{33}, and s_{13} are fitted by straight lines in the whole or partial ranges of $-1 < P_3^R/P_{3sat}^R < -0.5$ at room and high temperatures. In Fig. 3(a), d_{33} is fitted by a single quadratic curve for the whole range between $-1 < P_3^R/P_{3sat}^R < -0.5$; in Fig. 3(b), s_{33} and s_{13} are fitted by two quadratic curves, each of which is defined for $-1 < P_3^R/P_{3sat}^R < -0.75$ and $-0.75 < P_3^R/P_{3sat}^R < -0.5$, respectively. The fitting quadratic curves are given as functions of P_3^R/P_{3sat}^R by

$$\hat{d}_{33}(P_3^R) = a_{d33}\left(\frac{P_3^R}{P_{3sat}^R}\right)^2 + b_{d33}\left(\frac{P_3^R}{P_{3sat}^R}\right) + c_{d33},$$

$$\hat{s}_{33}(P_3^R) = a_{s33}\left(\frac{P_3^R}{P_{3sat}^R}\right)^2 + b_{s33}\left(\frac{P_3^R}{P_{3sat}^R}\right) + c_{s33},$$

$$\hat{s}_{13}(P_3^R) = a_{s13}\left(\frac{P_3^R}{P_{3sat}^R}\right)^2 + b_{s13}\left(\frac{P_3^R}{P_{3sat}^R}\right) + c_{s13}, \quad (1)$$

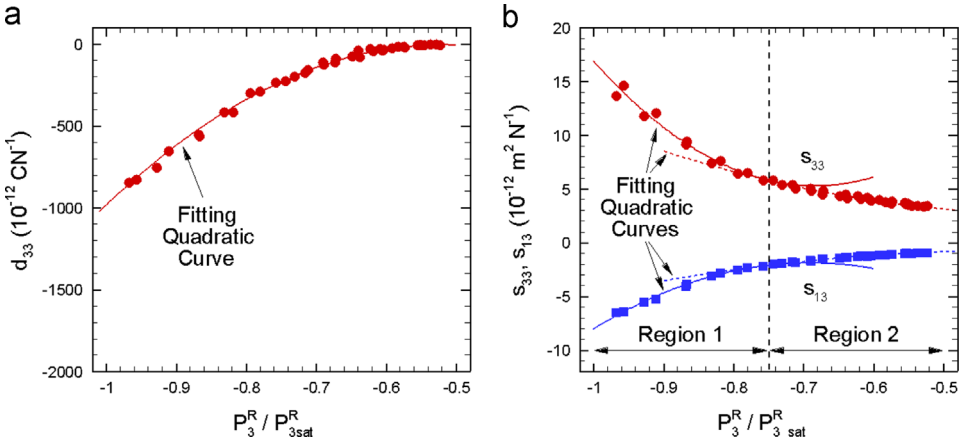

Fig. 3. Distribution of (a) piezoelectric coefficient d_{33} and (b) compliance coefficients s_{33}, s_{13} plotted versus relative remnant polarization P_3^R/P_{3sat}^R. Data points of d_{33} are fitted by one quadratic curve and those of s_{33}, s_{13} by two quadratic curves, for $-1 < P_3^R/P_{3sat}^R < -0.5$.

Table 1
Values of coefficients a, b, and c for linear material properties.

Linear material properties	Range of P_3^R/P_{3sat}^R	Coefficients		
		a	b	c
d_{33}[C N^{-1}]	$-1 < P_3^R/P_{3sat}^R < -0.50$	-4191.7×10^{-12}	-4332.1×10^{-12}	1119.9×10^{-12}
s_{33}[m^2 N^{-1}]	$-1 < P_3^R/P_{3sat}^R < -0.75$	115.2×10^{-12}	157.5×10^{-12}	59.13×10^{-12}
	$-0.75 < P_3^R/P_{3sat}^R < -0.50$	18.72×10^{-12}	12.75×10^{-12}	4.86×10^{-12}
s_{13}[m^2 N^{-1}]	$-1 < P_3^R/P_{3sat}^R < -0.75$	-64.18×10^{-12}	-88.61×10^{-12}	-32.42×10^{-12}
	$-0.75 < P_3^R/P_{3sat}^R < -0.50$	-10.89×10^{-12}	-8.46×10^{-12}	-2.29×10^{-12}

where a, b, and c, subscripted with the symbols of linear material properties, are constants for fitting quadratic functions. The units of a, b, and c are the same as those of associated linear material properties and their values are tabulated in Table 1. In next section, Eq. (1) will be used to calculate the evolutions of remnant state variables and linear material properties during compressive creep loading and unloading cycle.

3.2. Measured responses to compressive creep loading and unloading

The responses of a poled PZT specimen to compressive creep loading and unloading are measured. Applied compressive stress increases at a rate of -0.5 MPa s^{-1} up to eight different target levels of -20, -30, -50, -70, -100, -150, -300, and -500 MPa. After remaining 500 s at each constant target level, unloading starts abruptly at the same rate of 0.5 MPa s^{-1}. Then, the material responses at zero stress are measured for another 500 s. The responses during the total loading and unloading period of time are plotted in Fig. 4. Electric displacement D_3 and longitudinal and transverse strains S_3, S_1 are plotted versus stress T_3 in Fig. 4(a) and (b), respectively. Before loading starts, the value of D_3 is about -0.5 Cm^{-2} and the magnitudes of S_3 and S_1 are set to be zero. It is shown in the figures that the D_3–T_3 and S_3 (or S_1)–T_3 curves are saturated with increasing compressive stress. The evolutions of D_3, S_3, and S_1 are also plotted versus time in Fig. 4(c) and (d), respectively. As will be discussed in Fig. 4(e) and (f), the magnitude of induced electric displacement during loading is saturated as the magnitude of compressive stress increases; but those of induced strains increase constantly with compressive stress. The magnitude of recovered electric displacement during unloading is maximum near $T_3 = -50$ MPa, whereas those of recovered strains increase with increasing compressive stress. The magnitudes of induced and recovered electric displacement and strains during total loading and unloading periods of time that are obtained from Fig. 4(c) and (d) are plotted versus stress T_3 in Fig. 4(e) and (f), respectively. In Fig. 4(e), the magnitude of induced electric displacement during loading $(\Delta D_3)_l$ increases linearly with compressive stress below -100 MPa or so, but it is saturated with increasing compressive stress. The magnitude of electric displacement recovered during unloading $(\Delta D_3)_u$ is also plotted as empty circle symbols with dotted line segments in the figure. At relatively small magnitudes of compressive stress, $(\Delta D_3)_u$ increases linearly with compressive stress. But, after hitting maximum at about -60 MPa, it decreases gradually with stress. Similarly, in Fig. 4(f), the magnitudes of both induced strains during loading $(\Delta S_3)_l$, $(\Delta S_1)_l$ and recovered strains during unloading $(\Delta S_3)_u$, $(\Delta S_1)_u$ are plotted versus applied stress. It is seen that all of them increase rapidly at smaller compressive stress but slowly at larger compressive stress.

3.3. Evolution of material properties and remnant state variables during compressive creep loading and unloading

In order to calculate the evolutions of material properties and remnant state variables during compressive creep loading

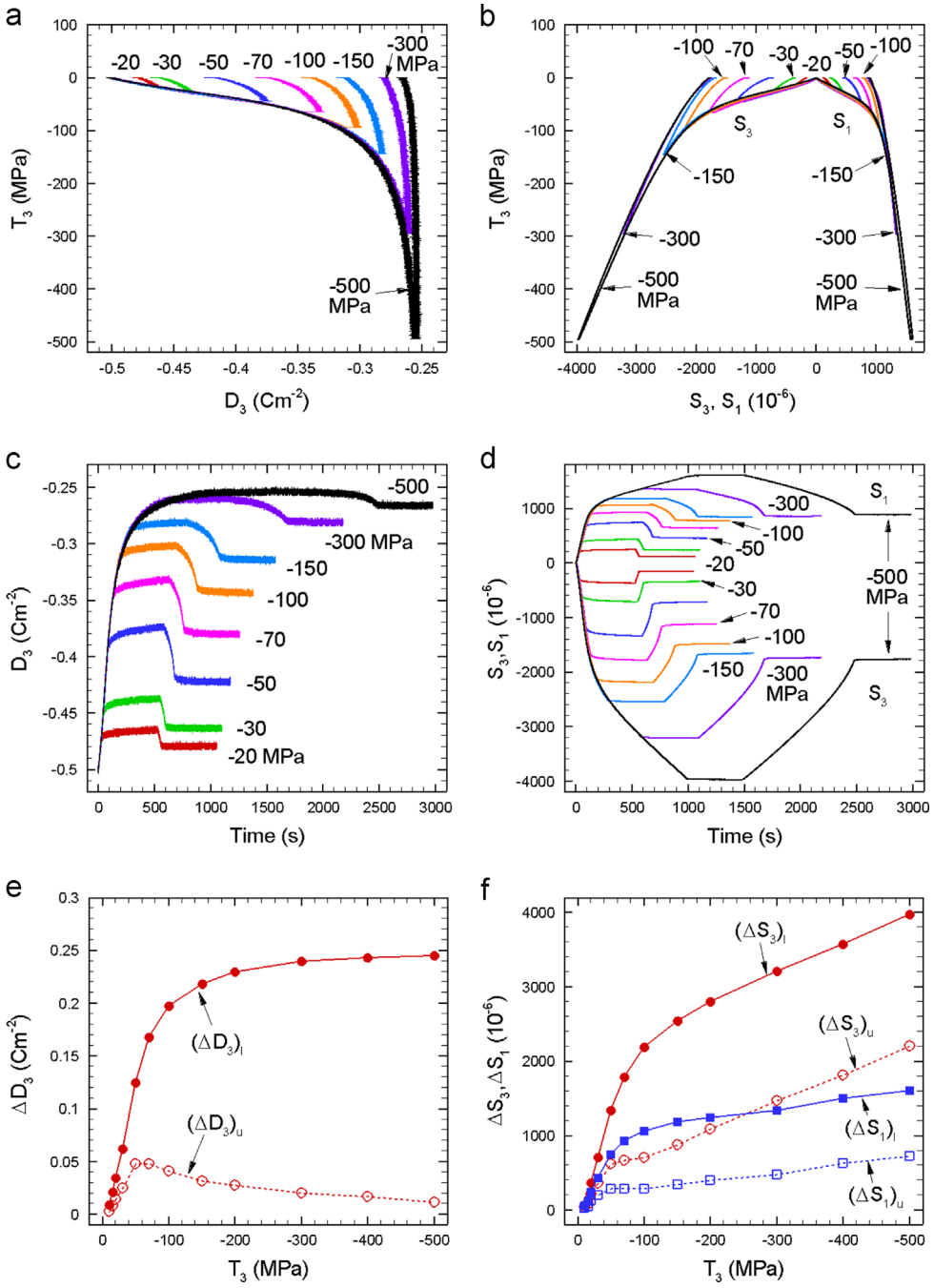

Fig. 4. Measured electric displacement and strains during compressive creep loading and unloading: (a) stress T_3 versus electric displacement D_3, (b) stress T_3 versus strains S_3, S_1, (c) electric displacement D_3 versus time, (d) strains S_3, S_1 versus time, (e) the magnitudes of induced electric displacement $(\Delta D_3)_l$ during loading and recovered electric displacement $(\Delta D_3)_u$ during unloading of compressive stress plotted versus stress T_3, and (f) the magnitudes of induced strains $(\Delta S_3)_l$, $(\Delta S_1)_l$ during loading and recovered strains $(\Delta S_3)_u$,$(\Delta S_1)_u$ during unloading of compressive stress plotted versus stress T_3.

and unloading, it is necessary to insert Eq. (1) into piezoelectric equations given by

$$\begin{aligned} D_3 &= d_{33}T_3 + P_3^R, \\ S_3 &= s_{33}T_3 + S_3^R, \\ S_1 &= s_{13}T_3 + S_1^R, \end{aligned} \tag{2}$$

where P_3^R is remnant polarization, S_3^R is the longitudinal remnant strain, and S_1^R is the transverse remnant strain. Inserting d_{33} from Eq. (1) into Eq.$(2)_1$, we get a second order equation of P_3^R given by

$$\frac{a_{d33}T_3}{(P_{3sat}^R)^2}(P_3^R)^2 + \left(\frac{b_{d33}T_3}{P_{3sat}^R} + 1\right)(P_3^R) + (c_{d33}T_3 - D_3 c_{d33}T_3 - D_3) = 0, \tag{3}$$

where P_{3sat}^R is the magnitude of remnant polarization at a saturated (poled) state, T_3 is the applied compressive stress, D_3 measured electric displacement, and a_{d33}, b_{d33}, and c_{d33} are the coefficients associated with d_{33} given in Table 1. After solving

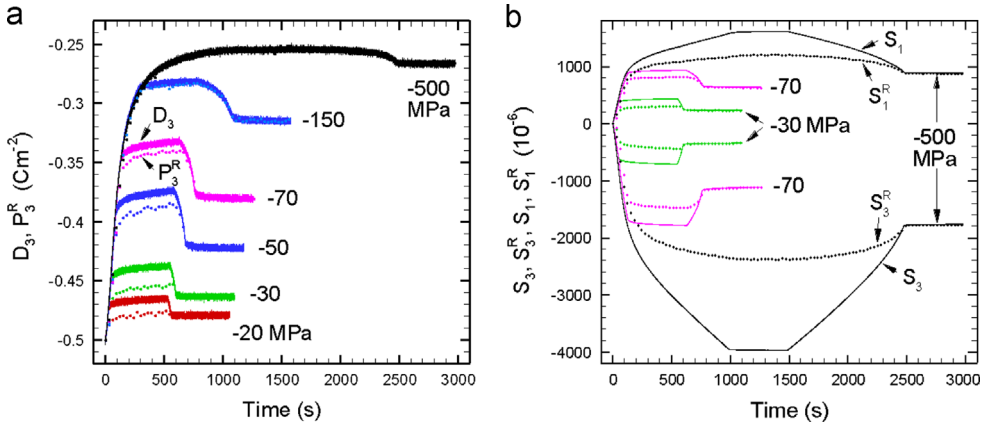

Fig. 5. Time evolution of (a) electric displacement D_3 and remnant polarization P_3^R and (b) strains S_3, S_1 and remnant strains S_3^R, S_1^R at various levels of compressive stress. D_3, S_3, and S_1 are represented by solid lines and P_3^R, S_3^R, and S_1^R by dashed ones.

Eq. (3) for remnant polarization P_3^R, it is inserted into Eq. $(1)_2$ and $(1)_3$ to obtain compliance coefficients $s_{33}$and s_{13}, respectively. Then, they are used in Eq. $(2)_2$ and $(2)_3$, yielding longitudinal and transverse remnant strains S_3^R and S_1^R, respectively.

In Fig. 5(a), the calculated P_3^R's are plotted versus time as dotted lines for six stress levels −20, −30, −50, −70, −150, and −500 MPa, and they are compared with measured electric displacement D_3. It is seen that P_3^R curves are always below D_3 curves. Difference between D_3 and P_3^R is negligibly small at relatively large compressive stresses −150 MPa and −500 MPa. It is because the degree of poling in the specimen is nearly vanished under the application of large compressive stress and the magnitude of piezoelectric coefficient d_{33} is saturated to zero at the large stresses, as shown in Fig. 6(a). The difference between D_3 and P_3^R is larger at smaller magnitudes of compressive stress, reaching maximum at −30 MPa in the figure. It is due to larger magnitude of d_{33} at smaller compressive stress, as shown in Fig. 6(a). Looking at Fig. 5(b), where measured strains S_3 and S_1 are plotted as solid lines and calculated remnant strains S_3^R and S_1^R as dotted lines, it is observed that the magnitudes of S_3^R and S_1^R are always smaller than those of S_3 and S_1. It is interesting that contrary to D_3 and P_3^R in Fig. 5(a), the difference between S_3^R and S_3 (or S_1^R and S_1) gets large with increasing compressive stress. It is because s_{33} and s_{13} approach certain nonzero finite values, instead of zero in d_{33}, with increasing compressive stress, as shown in Fig. 6(b).

In Fig. 7(a), the magnitudes of induced remnant polarization $(\Delta P_3^R)_l$ during loading period of compressive stress and recovered remnant polarization $(\Delta P_3^R)_u$ during unloading period, both obtained from Fig. 5(a), are plotted versus compressive stress as solid circle symbols and empty circle symbols, respectively. The curves of $(\Delta P_3^R)_l$ and $(\Delta P_3^R)_u$ in the figure are similar to those of $(\Delta D_3^R)_l$ and $(\Delta D_3^R)_u$ in Fig. 4(e). It is because the magnitude of d_{33} converges to zero with increasing compressive stress, as shown in Figs. 3(a) and 6(a). On the other hand, the magnitude of induced remnant longitudinal strain $(\Delta S_3^R)_l$ (or induced remnant transverse strain $(\Delta S_1^R)_l$) in Fig. 7(b) is much smaller than that of induced longitudinal strain $(\Delta S_3)_l$ (or induced transverse strain $(\Delta S_1)_l$) in Fig. 4(f). So does the magnitude of recovered remnant longitudinal strain $(\Delta S_3^R)_u$ (or recovered remnant transverse strain $(\Delta S_1^R)_u$) in Fig. 7(b) compared with that of recovered longitudinal strain $(\Delta S_3)_u$ (or recovered transverse strain $(\Delta S_1)_u$) in Fig. 4(f). It is because the magnitudes of compliance coefficients s_{33} and s_{13} have nonzero finite values even at the largest compressive stress in the figure, as clearly seen in Figs. 3(b) and 6(b). Comparing Fig. 7(a) and (b), it is seen clearly that the magnitude of $(\Delta P_3^R)_u$ decreases but those of $(\Delta S_3^R)_u$ and $(\Delta S_1^R)_u$ increase with increasing compressive stress. The ratios of the magnitude of induced remnant state variables during loading with respect to those of recovered remnant state variables during unloading of compressive stress are plotted in Fig. 7(c).$(\Delta P_3^R)_u/(\Delta P_3^R)_l$ is represented by solid circle symbols with solid line segments, $(\Delta S_3^R)_u/(\Delta S_3^R)_l$ by solid square symbols with dashed line segments, and $(\Delta S_1^R)_u/(\Delta S_1^R)_l$ by solid diamond symbols with long-dashed line segments. The three ratios hit the maximum value of about 0.32 near −50 MPa. Then they decrease equally with increasing compressive stress until −100 MPa. In the stress range, both remnant polarization and remnant strains are recovered in the same ratio during unloading. However, above −100 MPa, the case is different. The values of both $(\Delta S_3^R)_u/(\Delta S_3^R)_l$ and $(\Delta S_1^R)_u/(\Delta S_1^R)_l$ increase equally and gradually with increasing compressive stress, but that of $(\Delta P_3^R)_u/(\Delta P_3^R)_l$ decreases with stress. That is, the relative amounts of recovered remnant longitudinal and transverse strains increase, but that of recovered remnant polarization decreases, with compressive stress. During unloading of compressive stress, remnant polarization is recovered approximately in the same ratio as those of remnant longitudinal and transverse strains for smaller magnitude of compressive stress, but it is recovered in a much smaller ratio for larger magnitudes of compressive stress.

4. Conclusions

A poled PZT cube specimen is subjected to compressive stress in the poling direction. First, impulsive compression stress with increasing amplitude is applied at the fastest rate of 10 MPa s^{-1} available in the machine. Linear material

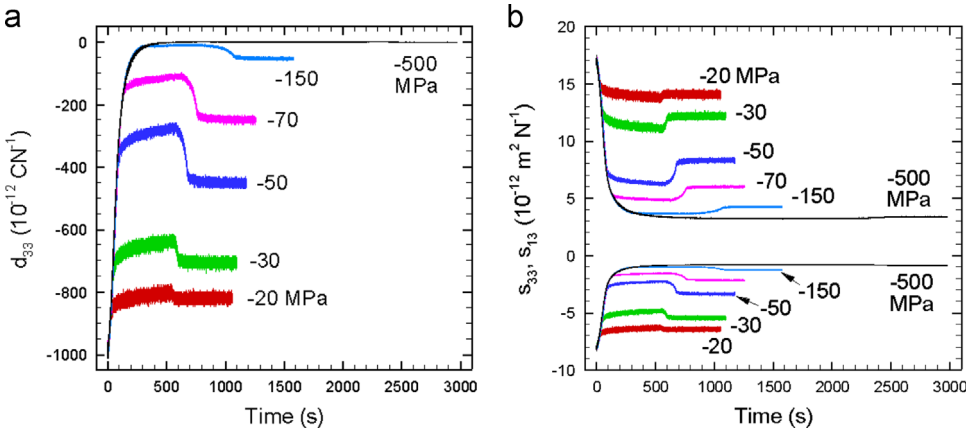

Fig. 6. Time evolution of (a) piezoelectric coefficient d_{33} and (b) compliance coefficients s_{33} and s_{13} at various levels of compressive stress.

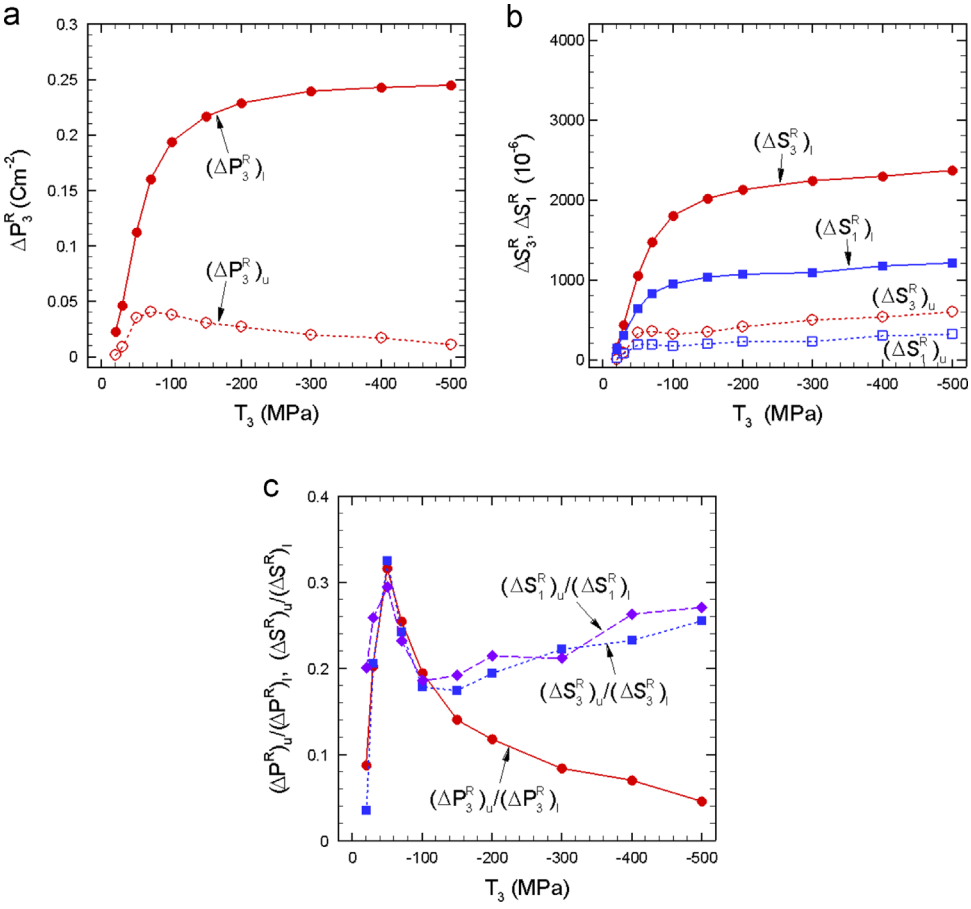

Fig. 7. Induced and recovered amounts of remnant state variables during loading and unloading of compressive stress, (a) the magnitudes of induced remnant polarization $(\Delta P_3^R)_l$ during loading and recovered remnant polarization $(\Delta P_3^R)_u$ during unloading of compressive stress plotted versus stress T_3, and (b) the magnitudes of induced remnant strains $(\Delta S_3^R)_l$, $(\Delta S_1^R)_l$ during loading and recovered remnant strains $(\Delta S_3^R)_u$ and $(\Delta S_1^R)_u$ during unloading of compressive stress plotted versus stress T_3, and (c) the ratios of recovered remnant variables with respect to induced remnant variables $(\Delta P_3^R)_u/(\Delta P_3^R)_l$, $(\Delta S_3^R)_u/(\Delta S_3^R)_l$, and $(\Delta S_1^R)_u/(\Delta S_1^R)_l$.

properties and remnant state variables are evaluated from measurements. Piezoelectric coefficient d_{33} shows a quadratic dependence on relative remnant polarization and it is fitted by a single quadratic curve for $-1 < P_3^R/P_{3sat}^R < -0.5$. Each of elastic compliance coefficients s_{33} and s_{13} is fitted by two quadratic curves for $-1 < P_3^R/P_{3sat}^R < -0.5$. The value of elastic Poisson's ratio is estimated to be 0.305 and that of switching-induced Poisson's ratio 0.476.

Then compressive stress of various magnitudes is applied and removed at the slow rate of 0.5 MPa s^{-1}. Applied stress is held constant for 500 s after both loading and unloading are finished. From measured electric displacement and strains,

remnant polarization and strains are calculated using the proposed quadratic dependence of linear material properties on relative remnant polarization. Remnant polarization is smaller than electric displacement for the compressive stresses smaller than −100 MPa or so, but no significant difference is observed for the compressive stresses larger than −100 MPa. On the contrary, the magnitudes of remnant strains are smaller than those of measured strains for all stress levels, the difference being greater at larger compressive stress. This opposite behavior of remnant polarization and strains is due to different convergent behavior of piezoelectric and compliance coefficients at large compressive stress. Piezoelectric coefficient converges to zero, but compliance coefficients to certain nonzero finite value, as the magnitude of compressive stress increases. It is interesting that the relative amount of recovered remnant polarization during unloading period of compressive stress decreases, but those of recovered remnant strains increase, with increasing compressive stress.

Acknowledgments

The research was supported by Basic Science Research Program through the National Research Foundation of Korea (NRF) funded by the Ministry of Education, Science and Technology (2013-020386).

References

[1] J.E. Huber, N.A. Fleck, Multi-axial electrical switching of a ferroelectric: theory versus experiment, Journal of the Mechanics and Physics of Solids 49 (2001) 785–811.
[2] S.J. Kim, A constitutive model for thermo-electro-mechanical behavior of ferroelectric polycrystals near room temperature, International Journal of Solids and Structures 48 (2011) 1318–1329.
[3] L.D. Mauck, C.S. Lynch, Thermo-electro-mechanical behavior of ferroelectric materials. Part I: a constitutive micromechanical model versus experimental results, Journal of Intelligent Materials Systems and Structures 14 (2003) 587–602.
[4] H. Cao, A.G. Evans, Nonlinear deformation of ferroelectric ceramics, Journal of American Ceramic Society 76 (1993) 890–896.
[5] C.S. Lynch, The effect of uniaxial stress on the electro-mechanical response of 8/65/35 PLZT, Acta Materialia 44 (1996) 4137–4148.
[6] T. Fett, G. Thun, Determination of room-temperature tensile creep of PZT, Journal of Materials Science Letters 17 (1998) 1929–1931.
[7] S.J. Kim, C.H. Lee, Creep behavior of a poled PZT wafer under longitudinal tensile stress and through thickness electric field, International Journal of Solids and Structures 46 (2009) 716–725.
[8] J.S. Forrester, E.H. Kisi, Ferroelastic switching in a soft lead zirconate titanate, Journal of European Ceramic Society 24 (2004) 595–602.
[9] D. Zhou, M. Kamlah, Room-temperature creep of soft PZT under static electrical and compressive stress loading, Acta Materialia 54 (2006) 1389–1396.
[10] T. Fett, D. Munz, G. Thun, Young's modulus of soft PZT from partial unloading tests, Ferroelectrics 274 (2002) 67–81.
[11] D. Zhou, R. Wang, M. Kamlah, Determination of reversible and irreversible contributions to the polarization and strain response of soft PZT using the partial unloading method, Journal of European Ceramic Society 30 (2010) 2603–2615.
[12] M. Selten, G.A. Schneider, V. Knoblauch, R.M. McMeeking, On the evolution of the linear material properties of PZT during loading history – an experimental study, International Journal of Solids and Structures 42 (2005) 3953–3966.
[13] Q.D. Liu, J.E. Huber., State dependent linear moduli in ferroelectrics, International Journal of Solids and Structures 44 (2007) 5635–5650.
[14] K.G. Webber, E. Aulbach, T. Key, M. Marsilius, T. Granzow, J. Rodel, Temperature-dependent ferroelastic switching of soft lead zirconate titanate, Acta Materialia. 57 (2009) 4614–4623.
[15] S.J. Kim, Y.S. Kim, State dependent pyroelectric and thermal expansion coefficients in a PZT wafer, Ceramics International 36 (2010) 2189–2196.
[16] Y.S. Kim, S.J. Kim, Evolution of linear moduli and remanent state variables during polarization reversal in a lead zirconate titanate wafer at various temperatures, Japanese Journal of Applied Physics 50 (2011) 031503.
[17] S.J. Kim, J.H. Kim, C.H. Lee, Domain switching and creep behavior of a poled PZT wafer under through-thickness electric fields at high temperatures, Acta Materialia 58 (2010) 2237–2249.
[18] N. Lee, S.J. Kim, Effects of loading rate and temperature on domain switching and evolutions of reference state variables during polarization reversal in a PZT wafer, Ceramics International 38 (2012) 1115–1126.
[19] D.W. Ji, S.J. Kim, Temperature-dependent ferroelastic switching of ferroelectric ceramics and evolution of linear material properties, Acta Materialia 61 (2013) 1–11.
[20] S.J. Kim, D.W. Ji, Temperature-dependent compressive creep of ferroelectric ceramics and evolution of remnant state variables, Journal of European Ceramic Society 33 (2013) 1779–1792.